Geophysical Journal International

Advanting Astronousy and Geophysics

Geophys. J. Int. (2021) 225, 1–14 Advance Access publication 2020 December 12 GJI Geomagnetism, rock magnetism and palaeomagnetism doi: 10.1093/gji/ggaa569

Magnetic hysteresis of magnetite, pyrrhotite and hematite at high temperature

David J. Dunlop

Department of Physics, University of Toronto, Toronto, ON M5S1A7, Canada. E-mail: dunlop@physics.utoronto.ca

Accepted 2020 November 24. Received 2020 November 13; in original form 2020 August 3

SUMMARY

The magnetic properties of iron-bearing minerals at above-ambient temperatures control their magnetic expression at depth in the Earth and other planets, as well as the permanent memory they retain as thermoremanence or thermochemical remanence when brought to the surface and cooled. This paper reports magnetic hysteresis parameters measured at temperatures up to the Curie point $T_{\rm C}$ for natural pyrrhotite and hematite and for suites of sized magnetites, both natural and synthesized. Domain structure changes can be inferred from the ratio of saturation remanence $M_{\rm rs}$ to saturation magnetization $M_{\rm s}$. In almost all magnetites and pyrrhotites studied, $M_{\rm rs}$ decreases more rapidly with increasing measurement temperature T than $M_{\rm s}$, indicating thermal unblocking or vortex development in single-domain grains and addition or remobilization of domain walls at high T in multidomain grains. During cooling of a rock, iron minerals might then denucleate domains or vortices. Coercive force $H_{\rm c}$, a measure of stability against changing magnetic fields, also decreases with increasing measurement T, usually at a rate similar to that of $M_{\rm rs}$, but often retains a finite value near the Curie point.

Key words: Magnetic mineralogy and petrology; Rock and mineral magnetism.

1 INTRODUCTION

The magnetic properties of the iron oxides and sulphides magnetite (Fe₃O₄), hematite (α Fe₂O₃) and monoclinic 4C pyrrhotite (Fe₇S₈) at above-ambient temperatures T govern their magnetic expression at depth in the Earth and other planets, fore example, Mars. They also determine the magnetic memory these minerals retain in the form of thermoremanent magnetization (TRM) or thermochemical remanence when they cool during uplift to the surface.

Initial susceptibility $k_0(T)$, which determines induced magnetization at depth, is routinely measured for palaeomagnetic samples but the higher-field parts of the hysteresis curve are rarely determined at elevated temperatures (Dunlop 1976, 1987; Dunlop & Bina 1977; Levi & Merrill 1978; Özdemir & O'Reilly 1981, 1982; Hartstra 1982a,b; Heider et al. 1987; Bina & Prévot 1989; Argyle & Dunlop 1990; Keller & Schmidbauer 1999; Yu et al. 2004), despite the usefulness of such data. For example, the hysteresis parameter $H_c(T)$ (coercive force), one measure of coercivity or resistance to field changes at temperature T, enters directly into Néel's (1955) theory of TRM acquisition and other theories based on it (Everitt 1962; Schmidt 1973; Dunlop & Xu 1994; Xu & Dunlop 1994; Berndt & Chang 2018). Another informative parameter is M_{rs}/M_s , the ratio of saturation remanence M_{rs} to saturation magnetization M_{s} , also known as the squareness. Knowing M_{rs}/M_s as a function of T, inferences can be made about possible changes of magnetic domain structure in the course of cooling or heating.

This paper reports high-temperature hysteresis data for selected samples of natural pyrrhotite, hematite and magnetite, as well as for sized fractions of magnetite obtained by crushing natural crystals and for a few synthesized magnetites. The room-temperature domain structures of the samples range from stable single-domain [SD; with variable amounts of admixed thermally unstable superparamagnetic (SP] material), to large multidomain (MD) with broad domains and narrow domain walls, through transitional states such as spin vortices and few-domain structures with broad walls. Some transitional states exhibit unexpectedly large H_c and $M_{\rm rs}/M_{\rm s}$ values, often referred to as pseudo-single-domain (PSD) behaviour (Stacey 1962, 1963; Roberts *et al.* 2017).

The purpose of the present paper is to establish the broad pattern of variations in H_c , $M_{\rm rs}$, $M_{\rm rs}/M_{\rm s}$ and domain structure with temperature. In the case of magnetite, these variations can be compared directly with published data for narrowly sized SD particles (Dunlop 1987). A more detailed analysis of grain-size and temperature variations in the suites of sized magnetites will appear in a separate paper.

2 EXPERIMENTAL METHODS AND SAMPLES

Measurements were made at the Institute for Rock Magnetism, University of Minnesota. Hysteresis loops of magnetization M versus magnetic field H were measured at 10 $^{\circ}$ C intervals from 25 to

325 °C for pyrrhotite, at 20 °C intervals from 25 to 565 or 585 °C for magnetite and at 20 °C intervals from 25 to 685 °C for hematite. The maximum available field of 1 T (\approx 800 kA m⁻¹) was insufficient to saturate any of the hematites. A field of 0.5 T served to saturate the remanence of all the magnetites and also pyrrhotite within its basal easy plane but not along the magnetically hard c-axis. The M-H-T measurement sequence was pre-programmed on a Princeton Measurements Corporation micro-VSM (vibrating-sample magnetometer). Complete major loops were measured at each T using field steps of 3, 5 and 10 mT for pyrrhotite, magnetite and hematite, respectively. After measuring a loop, the sample was heated in zero field to the next measurement temperature. Flowing He gas was used to inhibit oxidation of the pyrrhotite and magnetite samples while measuring at constant T and during heating. A complete set of measurements required about 6 hr, including a repeat run at 25 °C after cooling from peak temperature.

As part of the sample selection process, natural hematites and pyrrhotites were tested for purity with a Geofyzika KLY-2 Kappabridge variable-temperature AC susceptibility bridge, which uses a 920 Hz alternating field ($H=0.3~\rm kA~m^{-1}~rms$). Measurements of initial susceptibility $k_0(T)$ were recorded every $\approx 3~\rm ^{\circ}C$ during heating from 20 to 600 or 700 $\rm ^{\circ}C$ and cooling back to 50 $\rm ^{\circ}C$. A complete heating-cooling run took about 2 hr. A stream of Ar gas was used to inhibit oxidation of the pyrrhotites but many nevertheless displayed minor peaks around the 580 $\rm ^{\circ}C$ magnetite Curie point.

Natural hematite crystals came from localities in Canada, USA and Italy (Elba). Minute amounts of magnetite were a persistent contaminant, made prominent in the magnetic results by the 200 times contrast in spontaneous magnetizations ($\approx\!500~kA~m^{-1}$ for Fe $_3O_4$, $\approx\!2.5~kA~m^{-1}$ for αFe_2O_3). Chemically synthesized fine-particle hematites were generally magnetite-free but their coercivities extended much above the 1-T maximum field of the electromagnet and no meaningful hysteresis curves could be obtained.

Pyrrhotites from mines or mineral localities in Canada, USA and Mexico were tested. Only crystals from the Santa Eulalia mine (Chihuahua, Mexico) displayed a Hopkinson peak in $k_0(T)$ at 310–320 °C, just below the 325 °C Curie temperature of monoclinic pyrrhotite, and no indication of any other mineral. All the other pyrrhotites tested contained varying amounts of ferrimagnetic hexagonal pyrrhotite (Fe₉S₁₀ or Fe₁₁S₁₂; *cf.* Schwarz 1975) or magnetite, either present originally or produced during heating.

Massive magnetite ores from Marmora, Ontario (Canada) and Ishpeming, Michigan (USA) and single crystals from Bancroft, Ontario (Princess Quarry, PQ) were sources of MD magnetite. Some of the PQ crystals were crushed with mortar and pestle and sieved into two coarse-grained fractions. The residue was separated with a Bahco centrifugal dust analyser into seven finer-grained fractions, with mean sizes ranging from <1 to $20~\mu m$ (see Dunlop $\it et al. 2018$ for size distributions).

Two mineral separates from the Matachewan diabase (Ontario, Canada) were studied (see Dunlop *et al.* 2005). The first is a plagioclase separate from diabase sample TK49 containing fine magnetite inclusions with SD hysteresis properties at room temperature: $M_{\rm rs}/M_{\rm s}=0.455,~\mu_0H_{\rm c}=53.6~{\rm mT}$ (Table 1). The second, a dark minerals separate from sample TK128, contains magnetite with large PSD to small MD hysteresis at 20 °C: $M_{\rm rs}/M_{\rm s}=0.029,~\mu_0H_{\rm c}=3.1~{\rm mT}.$

A magnetite sample, FH3A, prepared using a low-temperature hydrothermal procedure (Heider *et al.* 1987), was included in the study as a representative of magnetites with low levels of internal stress. The grain-size spectrum peaks near 3 μ m but tails off to smaller sizes.

Table 1. Magnetite grain sizes and room-temperature hysteresis parameters after heating run 1.

Sample	Grain size (µm)	$M_{\rm rs}/M_{\rm s}$	$\mu_0 H_c \text{ (mT)}$
Wright 4000	0.025-0.065	0.195	16.7
TK49 plagioclase		0.455	53.6
Wright 112978	0.19 - 0.44	0.278	22.5
Wright 5000	0.34-0.75	0.249	23.4
Wright 3006	1.0-1.1	0.203	19.5
0.6 U	av. 0.62	0.180	16.4
1 U	av. 0.96	0.148	12.6
3 A	av. 3.0	0.115	11.2
3 U	av. 3.0	0.101	10.0
6 U	av. 5.8	0.093	8.6
FH3A hydrothermal	≤ 3	0.089	9.1
9 U	av. 8.9	0.079	7.7
14 U	av. 14.1	0.068	6.4
20 U	av. 20.0	0.047	6.2
Wright 041183	18.3-40	0.040	4.2
TK128 dark minerals		0.029	3.1
Wright 112982	16.9-37.5	0.026	2.8
110 U	100-125	0.014	2.8
135 U	125-150	0.009	1.35
Ishpeming ore		0.007	0.9

To add information in grain size/domain state intervals not well covered by the PQ and other natural magnetites, a number of synthesized magnetites from the Wright Company were studied as well. These have been included in several previous studies (Jackson *et al.* 1990; Yu *et al.* 2002, 2004; Carter-Stiglitz *et al.* 2006). However, information is scant about origin/method of preparation of the various powders and the reported average grain sizes are contradictory, perhaps referring to lots produced in different years. The Wright samples used in the present study are arranged in Table 1 according to their hysteresis parameters, principally $M_{\rm rs}/M_{\rm s}$ The grain size ranges are as given by the manufacturer.

The sized magnetites (PQ, FH3A, Wright) were dispersed as uniformly as possible in high-temperature alumina cement. Particle interaction remains a problem, particularly with the finer particles which tend to clump. Previous studies, for example, Yu *et al.* (2004), have shown that the hysteresis parameters of dispersed grains often do not differ much from those of bulk material.

3 MEASURED HYSTERESIS LOOPS

Room-temperature and high-temperature hysteresis loops characteristic of various domain states appear in Fig. 1. Flakes of massive hematite from Hoyt Lake, Minnesota (USA) exhibit a constricted or wasp-waisted minor loop at 20 °C (Fig. 1a), indicative of mixed magnetically soft and hard phases. Preferred orientation of the hematite flakes could conceivably produce loop constriction: at and above room temperature, the magnetization is confined to the basal c-plane of platy hematite crystals, while the trigonal c-axis has much higher anisotropy (Néel & Pauthenet 1952). However, high-temperature results described in the next section show that the lower-coercivity phase is magnetite. Its coercivity spectrum extends to ≈ 150 mT, marked by changes in slope in both ascending and descending branches of the loop. Hematite's c-plane coercivities extend well beyond the maximum 1000 mT driving field used to measure hysteresis. The hematite flakes are probably polycrystalline with a crystallite size below the SD threshold size d_0 , which depending on crystallinity is variously determined to be 0.5-2 µm

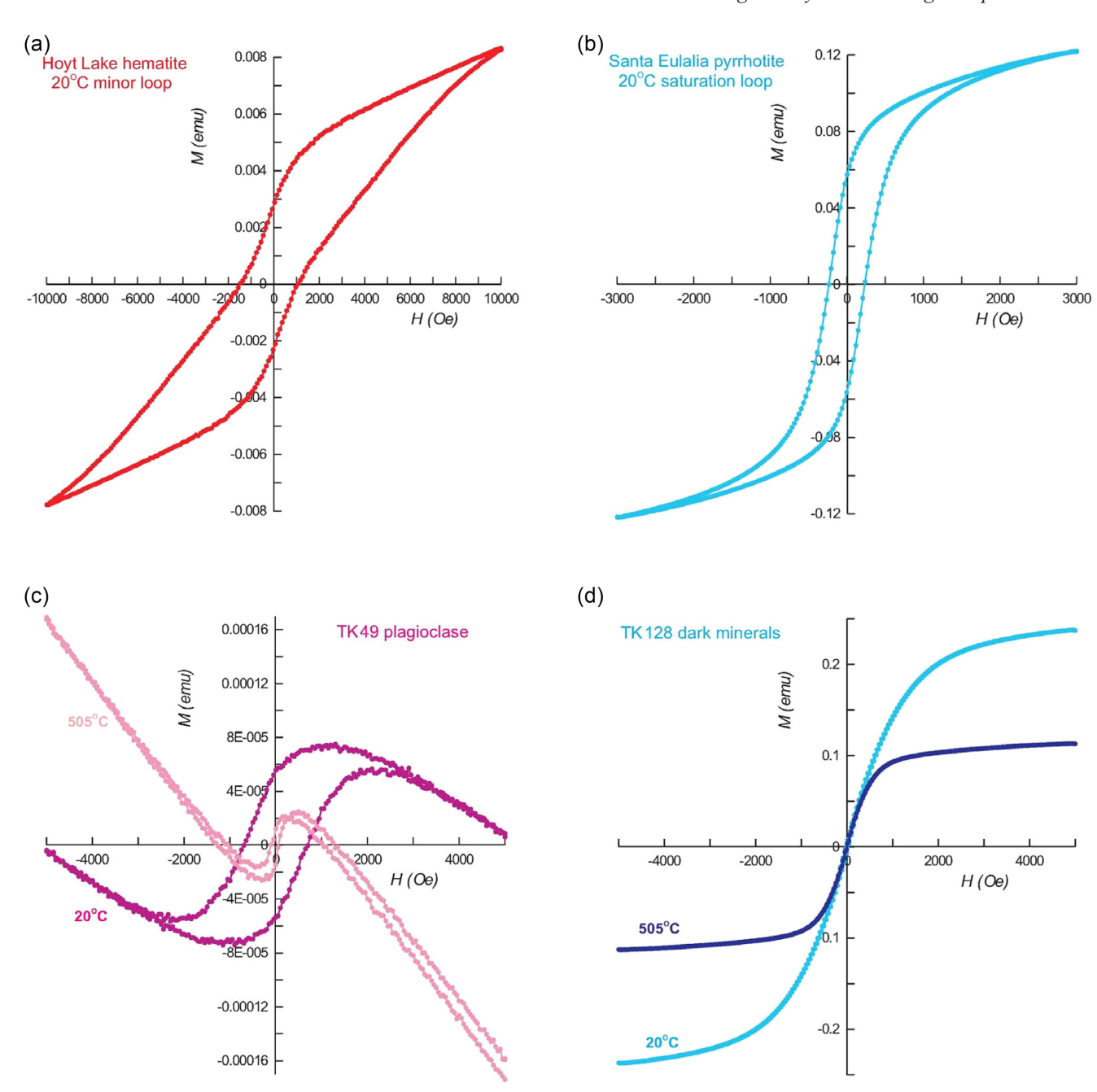


Figure 1. Hysteresis loops for selected samples, not corrected for paramagnetism or diamagnetism. (a) A wasp-waisted loop for the Hoyt Lake hematite ore, showing contamination of high-coercivity hematite by low-coercivity magnetite. (b) A single-domain (SD) loop measured at 20 °C for the Santa Eulalia pyrrhotite. Higher-temperature loops are less SD-like and have progressively lower remanence ratios $M_{\rm rs}/M_{\rm s}$. (c) Magnetite inclusions in TK49 plagioclase have SD hysteresis at 20 °C ($M_{\rm rs}/M_{\rm s}=0.455$) but most SD grains are unblocked by thermal fluctuations and become superparamagnetic (SP) by 505 °C. (d) Ramp-shaped hysteresis loops for small multidomain (MD) size (20–40 µm) magnetite inclusions in TK128 dark minerals separate. The slope of the central ramp is dictated by self-demagnetization. Note on units: 1 emu = 10^{-3} Am²; 1 Oe = 79.6 Am⁻¹; the equivalent *B* is 10^{-4} T.

(Dekkers & Linssen 1989), from 3–5 µm to 10–15 µm (Chevallier & Mathieu 1943; Banerjee 1971; Özdemir & Dunlop 2014) or ≥ 100 µm (Eaton & Morrish 1969; Kletetschka & Wasilewski 2002).

Small grains of Santa Eulalia pyrrhotite (Fig. 1b) a few tens of μ m in size display single-domain behaviour at 20 °C. The loop closes around 250 mT but continues to curve up to 500 mT, the maximum field used. Pyrrhotite crystallites whose hard c-axes lie close to the field direction cause this non-saturation. Pyrrhotite, like hematite, has high c-axis anisotropy compared to the anisotropy within the

easy c-plane (Bin & Pauthenet 1963; Schwarz 1975; Charilaou et~al. 2015). Standard high-field slope correction (using fields ≥ 70 per cent of the maximum field applied) yielded $M_{\rm rs}/M_{\rm s}=0.575$, in the range 0.5–0.637 for SD grains with uniaxial anisotropy and an easy plane of magnetization (Dunlop & Özdemir 1997, p. 321). Coercive force $\mu_0 H_c = 24.1$ mT, which corresponds to a nominal grain size of 30–40 μ m (Clark 1984; Dekkers 1988). The critical SD size d_0 of monoclinic pyrrhotite is much smaller than this, lying in the range 0.7–5 μ m (Soffel 1977; Clark 1984; Menyeh & O'Reilly 1996; Dunlop & Özdemir 1997, table 5.1; Wehland et~al. 2005) or

even smaller: 30–215 nm based on the sizes of coherent scattering domains observed in X-ray diffraction (Koulialias *et al.* 2019a). The Santa Eulalia pyrrhotite grains must therefore be polycrystalline.

The hysteresis loops of the TK49 plagioclase separate (Fig. 1c) have not been slope corrected for the diamagnetism of the plagioclase matrix and the quartz sample holder, which at the higher fields gives a signal at least as strong as that of the ferrimagnetic magnetite inclusions. The corrected ferrimagnetic loop has SD hysteresis at 20 °C with $M_{\rm rs}/M_{\rm s}\approx 0.5$, as noted in the previous section and in Table 1. However, at 505 °C the loop has contracted along both axes and $M_{\rm rs}/M_{\rm s}$ is well below 0.5. An exact value is difficult to determine because the loop does not close, probably as a result of minor temperature drift, but evidently some of the magnetite inclusions are no longer thermally stable SD but have become superparamagnetic (SP). This process of thermal unblocking reduces both $M_{\rm rs}/M_{\rm s}$ and $H_{\rm c}$. The mixture of hard SD and soft SP phases can result in wasp-waisted behaviour, although this is difficult to judge from an unclosed loop.

The hysteresis loops of the TK128 dark minerals separate owe their high-field slopes to paramagnetic minerals like biotite, actinolite and hornblende. The room-temperature ascending branch forms a gentle curve. There is minimal hysteresis between the ascending and descending branches. The hysteresis parameters after slope correction, $M_{\rm rs}/M_{\rm s}=0.029$ and $\mu_0H_{\rm c}=3.1$ mT, are those of large PSD/small MD magnetite in the approximate size range 20-40 μm (Table 1). At 505 °C, the central part of the *M*—*H* curve approaches a linear ramp, characteristic of larger MD grains with domain-wall motion limited by the internal demagnetizing field -NM, where N is the demagnetizing factor determined by the shape and domain configuration of each individual grain. This change in domain behaviour is likely due to increased wall mobility at higher T, not to grain growth. The inverse of the ramp slope gives an estimate of the average N value for the assemblage of magnetite inclusions. In this case, $N_{\rm av} \approx 0.175$ (SI) or 2.2 (cgs), corresponding to an average grain elongation of about 40 per cent. A detailed analysis of demagnetizing factors will appear in a separate paper.

4 HYSTERESIS LOOP PARAMETERS AS A FUNCTION OF TEMPERATURE

Fig. 2 illustrates how the hysteresis loop parameters $M_{\rm s}$, $M_{\rm rs}$ and $H_{\rm c}$ change as measurement temperature T increases for the four samples considered in the previous section. In the case of the Hoyt Lake hematite, it is only above $\approx 300~{}^{\circ}{\rm C}$ that the loops begin to approach saturation in a 1-T field and the parameters approximate those that would be measured in a saturating field. The effect of non-saturation of hematite on thermomagnetic curves has been described by de Boer & Dekkers (1998).

The increases in $M_{\rm s}$, $M_{\rm rs}$ and $H_{\rm c}$ of the Hoyt Lake hematite in temperature steps up to 250 °C (Fig. 2a) are the result of the changing shape of the measured minor loops. As coercivities decrease with heating and more of the coercivity spectrum becomes accessible to the 1-T maximum field, the loops become more rectangular. Above 250 °C, $H_{\rm c}$ changes more rapidly than $M_{\rm s}$ or $M_{\rm rs}$ and shows the clearest signature of magnetite. As the contaminating magnetite is progressively demagnetized in the 525, 545 and 565 °C steps, $H_{\rm c}$ rebounds to a peak at 585 °C. Thereafter $H_{\rm c}$ decreases steadily up to the 665 °C step but remains at a finite value in the 685 °C step instead of dropping to zero like $M_{\rm s}$ and $M_{\rm rs}$ $M_{\rm s}(T)$ has a strong inflection at the magnetite Curie point but $M_{\rm rs}(T)$ shows no obvious sign of magnetite. There is a striking contrast between the $M_{\rm rs}(T)$

and $H_{\rm c}(T)$ temperature dependences. This difference stems from the fact that hematite dominates the remanence and controls $M_{\rm rs}(T)$ while the magnetite has soft MD behaviour, with small remanence but large susceptibility k_0 and induced magnetization $M_{\rm in}=k_0H$. $H_{\rm c}$ measures a balance point—it is the field value H at which negative $M_{\rm in}$ in a reverse field -H cancels the positive $M_{\rm rs}$ of hematite. $H_{\rm c}$ is therefore strongly decreased by even very small amounts of soft magnetite.

 $M_s(T)$ measured in 10 °C steps for the Santa Eulalia pyrrhotite sample (Fig. 2b) gives a close approximation to the standard temperature variation of spontaneous magnetization of monoclinic 4C pyrrhotite (Dunlop & Özdemir 1997, fig. 3.27). The Curie temperature $T_{\rm C}$ is close to 325 °C. $M_{\rm rs}$ and $H_{\rm c}$ change in similar ways in measurement steps up to \approx 200 °C, then diverge. $M_{\rm rs}$ decreases at a steady rate between 255 and 305 °C, then vanishes at 325 °C like M_s H_c , on the other hand, decreases most between the 245 and 255 °C steps, after which the $H_c(T)$ curve has an inflection point and drops less rapidly, almost levelling out between 315 and 325 °C. In the final measurement step, although $M_{\rm s}$ and $M_{\rm rs}$ are almost zero, the loop has a finite width and H_c is about 7 per cent of its room-temperature value. At first sight this result seems to suggest a contaminant mineral with small M_s but large H_c , that is, hematite, but fine-grained magnetite produced by oxidation of the pyrrhotite is more likely.

The SD-size (at room temperature) magnetic inclusions in the TK49 plagioclase separate are close to magnetite in composition but contain a small amount of Ti or another cation, lowering the Curie temperature $T_{\rm C}$ from 580 °C to \approx 550 °C (Fig. 2c). Oxidation (maghemitization) of the magnetite would have the effect of raising rather than lowering $T_{\rm C}$ (Nishitani & Kono 1983). Because the concentration of (near-)magnetite is small, the hysteresis loops are noisy (Fig. 1c) and the determinations of H_c and M_{rs} and even M_s are not very precise. Nevertheless $M_s(T)$ has the general form expected for magnetite (cf. Dunlop & Özdemir 1997, fig. 3.5). M_{rs} decreases more rapidly with T than does M_s , with the result that M_{rs}/M_s drops below the stable SD value of 0.5 at higher T. This is as expected: the critical size for the onset of superparamagnetism (SP) or thermal instability of SD magnetic moments rises with increasing T (Néel 1949) and the smaller SD magnetic inclusions pass from a stable SD to an unstable SP state with zero remanence (Dunlop 1973). H_c is also affected by SP instability as T increases (Dunlop & Bina 1977; Dunlop & Özdemir 1997, eq. 8.24) and decreases even more rapidly with T than M_{rs}

The magnetite associated with the dark minerals in TK128 has the expected Curie point of $\approx 580~^{\circ}\mathrm{C}$ and $M_{\mathrm{s}}(T)$ values that are reproducible from one run to another (Fig. 2d). However, its other magnetic properties change after the first heating run. As a result of chemical and/or microstructural changes to the magnetite grains, the room-temperature values of M_{rs} and H_{c} increase by about 10 per cent after cooling from 585 °C at the conclusion of the first set of hysteresis measurements. In run 2, the M_{rs} and H_{c} data decrease in a more regular fashion than in run 1, where M_{rs} and H_{c} drop quite rapidly between 150 and 200 °C, then at a decreasing rate up to 350 °C. Above 350 °C, values from the two runs merge, suggesting that physiochemical changes to the magnetite were complete at this point in the original heating.

In both runs, the normalized $M_{\rm rs}(T)$ and $H_{\rm c}(T)$ curves are similar. This is an expected feature of MD behaviour because the ramplike ascending and descending branches of the hysteresis curve (e.g. Fig. 1d, 505 °C curve) have a slope of 1/N, where N is demagnetizing factor. Hence between the axis-crossing points on either branch, $M_{\rm rs}=(1/N)\,H_{\rm c}$. Since N is temperature independent,

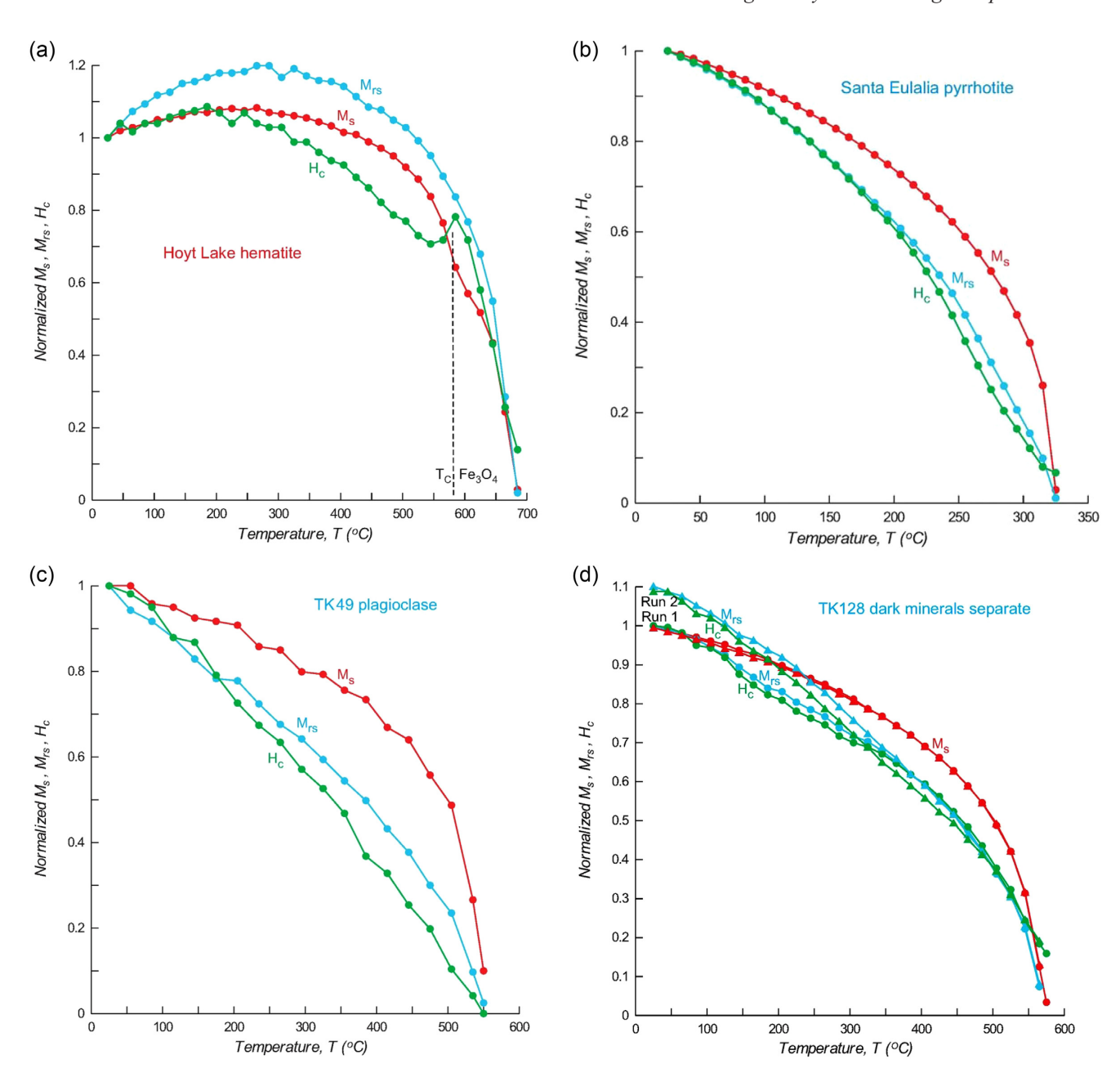


Figure 2. Normalized hysteresis parameters M_s , M_{rs} and H_c as a function of temperature T. (a) M_s and H_c data reveal the presence of magnetite with $T_C = 580$ °C in the Hoyt Lake hematite. (b) In the Santa Eulalia pyrrhotite, M_{rs} and H_c values decrease more rapidly with T than M_s . Above 165 °C, H_c drops faster than M_{rs} , suggesting thermal activation and unblocking of SD grains. (c) TK49 plagioclase also shows signs of thermal activation over a broad temperature range. M_{rs} and H_c decrease rapidly compared to M_s (almost linearly for H_c) from 20 to 550 °C and H_c drops faster than M_{rs} above 185 °C. (d) In TK128 dark minerals separate, M_{rs} and H_c have almost identical T variations, which stabilize only in the second heating run. Both parameters decrease more rapidly with T than M_s

 $M_{\rm rs}(T) \sim H_{\rm c}(T)$. As discussed in the previous section, the TK128 magnetite is only truly MD at the higher temperatures and has small MD/large PSD behaviour at 20 °C (Fig. 1d, Table 1). Despite this evolution of domain structure with temperature, the hysteresis curve is sufficiently linear and dominated by self-demagnetization between the axis crossings at H=0, $M=M_{\rm rs}$ and $H=-H_{\rm c}$, M=0 to preserve approximate proportionality between $M_{\rm rs}$ and $H_{\rm c}$ at lower as well as higher T. Note, however, that as in Figs 2(a) and (b) the $M_{\rm rs}(T)$ and $H_{\rm c}(T)$ curves diverge at the highest temperatures, beginning here at the 545 °C step. At 585 °C, where both $M_{\rm rs}$

and $M_{\rm s}$ approach zero, $H_{\rm c}$ retains about 15 per cent of its value at 20 °C.

5 CHANGES IN M_{rs}/M_s AND DOMAIN STRUCTURE WITH TEMPERATURE

The squareness ratio $M_{\rm rs}/M_{\rm s}$ is an indicator of domain structure. Fig. 3 compares $M_{\rm rs}/M_{\rm s}$ values measured at various temperatures for the four natural mineral samples of the previous two sections and two

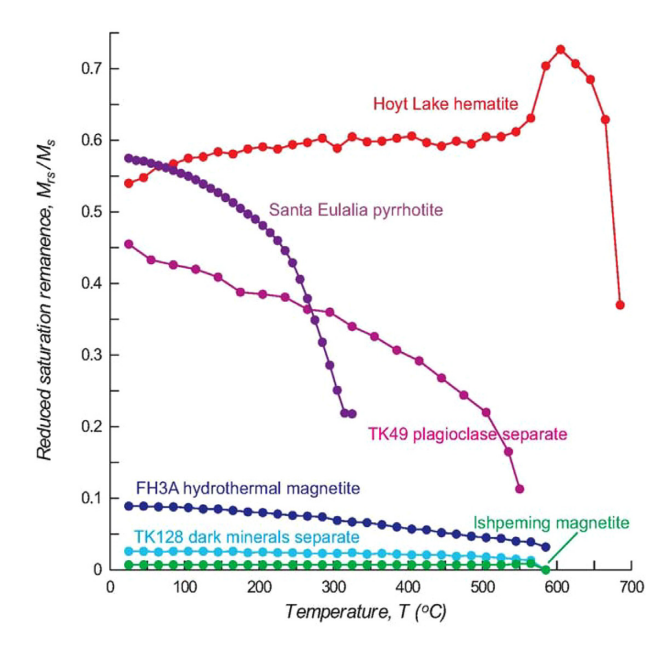


Figure 3. Evolution of the remanence ratio or squareness $M_{\rm rs}/M_{\rm S}$ in high-T hysteresis steps. True hematite values of $M_{\rm rs}/M_{\rm S}$ for the Hoyt Lake sample emerge only at 600 °C, above the magnetite Curie point. Both the Santa Eulalia pyrrhotite and TK49 (magnetite inclusions in plagioclase) exhibit strongly decreased remanence carrying capacity at higher T, characteristic of thermal unblocking of SD grains over a broad temperature range. PSD (pseudo-single-domain) to MD size magnetites FH3A and TK128 show slower but still continuous decreases of $M_{\rm rs}/M_{\rm s}$ values in higher T steps.

additional samples, the hydrothermally synthesized $< 3 \mu m$ magnetite FH3A and the Ishpeming magnetite ore, which has the most truly MD behaviour of all the magnetites (*cf.* Table 1).

Hematite is unusual in that M_{rs}/M_s is not an unambiguous domain state discriminator: $M_{rs}/M_s = 0.5-0.9$ for MD hematites, while $M_{\rm rs}/M_{\rm s} = 0.5 - 0.7$ for SD hematites (mostly unsaturated, i.e. minor loops; Özdemir & Dunlop 2014). The reason for the high MD values of $M_{\rm rs}/M_{\rm s}$ is the weak spontaneous magnetization of hematite, 200 times weaker than that of magnetite. The internal demagnetizing field -NM, which shears or inclines the M—H loop of MD magnetite, making M_{rs}/M_s small, has a negligible effect on the M—H loop of MD hematite. M_{rs}/M_s of the Hoyt Lake hematite increases slowly with increasing measurement temperature, from 0.54 at 20 °C to 0.62 at 545 °C, reflecting closer approach to saturation hysteresis. With removal of the signal of magnetite from 565-585 °C, M_{rs}/M_s rises to a peak of 0.72 at 605 °C, then begins to drop in the next four temperature steps. $M_{\rm rs}/M_{\rm s}=0.37$, about one-half the peak value, even at 685 °C, slightly above the nominal Curie point of hematite. Judging by the Curie points determined for the magnetite and pyrrhotite samples, the 685 °C temperature reading is believed to be accurate to within \pm 5 °C.

The Santa Eulalia pyrrhotite has SD behaviour ($M_{\rm rs}/M_{\rm s}=0.575$; cf. Dunlop & Özdemir 1997, p. 321) at room temperature, implying crystallites smaller than the SD threshold size. $M_{\rm rs}/M_{\rm s}$ decreases rapidly with quite mild heating, suggesting that some of the SD grains may be developing incoherent spin structures like vortices. Above the elbow around 230 °C, the decreasing values of $M_{\rm rs}/M_{\rm s}$ could be due to thermal unblocking, with grains passing from stable SD or vortex states to SP and losing their remanence.

On the other hand, this is also the T range in which diffusion of Fe²⁺ cations between alternating vacancy-poor and vacancy-rich c-planes becomes significant, ultimately equalizing vacancy populations on all cation layers (1C superstructure) and destroying the 4C vacancy ordering superstructure at $T_{\rm C} = 325$ °C (Koulialias et al. 2019b). Possibly the 1C superstructure with randomly distributed vacancies is attained in certain grains before others, or in portions of individual grains. Since 1C pyrrhotite has $M_s = 0$, M_{rs} of the ensemble of grains would then decrease. Textural effects due to cation migration, for example, diminishing size of X-ray coherent 4C domains (Koulialias et al. 2019a), might also promote magnetic changes, specifically the development of incoherent spin microstructures like corner flowering or internal full or partial vortices. Note, however, that substantial numbers of grains remain in a blocked SD state right up to $T_{\rm C}$. $M_{\rm rs}/M_{\rm s}$ levels out at ≈ 0.2 in the 315 and 325 °C steps, the T range of maximum cation migration. H_c reaches a plateau in the same interval (Fig. 2b).

The continuous drop of $M_{\rm rs}/M_{\rm s}$ values for the initially SD TK49 plagioclase separate, from 0.455 at room temperature to ≈ 0.1 at 545 °C, must be due to thermal unblocking. The stable SD range between the SP threshold size $d_{\rm s}$ and the SD \rightarrow vortex transition size $d_{\rm 0}$ is quite narrow in magnetite: 0.025–0.03 μ m to 0.05–0.06 μ m (Dunlop 1973; Dunlop & Özdemir 1997, table 5.1). As T increases, $d_{\rm s}$ grows rapidly towards $d_{\rm 0}$ (Dunlop & Özdemir 1997, eq. 8.27) and only the larger SD grains can remain blocked or thermally stable.

In the micrometre-size magnetite grains in sample FH3A, both spin vortices (Harrison *et al.* 2002; Almeida *et al.* 2014, 2016) and 2- or 3-domain structures with broad walls (Pan *et al.* 2002; Dunlop & Özdemir 2015, fig. 10) are likely to occur. The remanence associated with either will be stable to higher temperatures than that of SD grains, simply because much larger volumes of coupled spins must be thermally activated. For this reason, the long steady decline of $M_{\rm rs}/M_{\rm s}$ in FH3A probably indicates nucleation of more vortices or additional domains per grain at higher temperatures rather than thermal unblocking.

The large MD grains of the Ishpeming magnetite come closest to having a perfectly constant (low) value of $M_{\rm rs}/M_{\rm s}$ with changing T, indicating an unvarying equilibrium domain structure at all temperatures.

The $M_{\rm rs}/M_{\rm s}$ data for all the magnetites studied are displayed on a logarithmic scale in Fig. 4. Because most of the samples have relatively low M_{rs}/M_s values, a logarithmic plot spreads the data and brings out similarities and contrasts in the behaviour of different families of samples. It is also now clear to the eye that the two coarsest MD magnetites, the 135 µm crushed and sieved grains and the Ishpeming massive ore, do indeed have M_{rs}/M_s values that scarcely change with temperature and actually rise in the final steps before the Curie point, where all other samples have falling $M_{\rm rs}/M_{\rm s}$ values. In general, the finer the grain size the more rapid the decline in M_{rs}/M_s at elevated temperatures, that is, the more the domain structure changes. But even samples whose grain sizes approach the true MD range, TK128 dark minerals and Wright 041183 and 112982 magnetites (Table 1), have slowly but continuously declining values of $M_{\rm rs}/M_{\rm s}$ at moderate and high temperatures. They too alter their domain structure.

The two SD magnetite samples, TK49 plagioclase and Wright 4000, are in contrast to the other samples in showing clear signatures of thermally activated remanence unblocking. TK49 has been discussed above. Wright 4000, whose nominal grain sizes of 25–65 nm bracket the stable SD range of magnetite at room temperature, has a rapidly descending $M_{\rm rs}/M_{\rm s}(T)$ curve that cuts

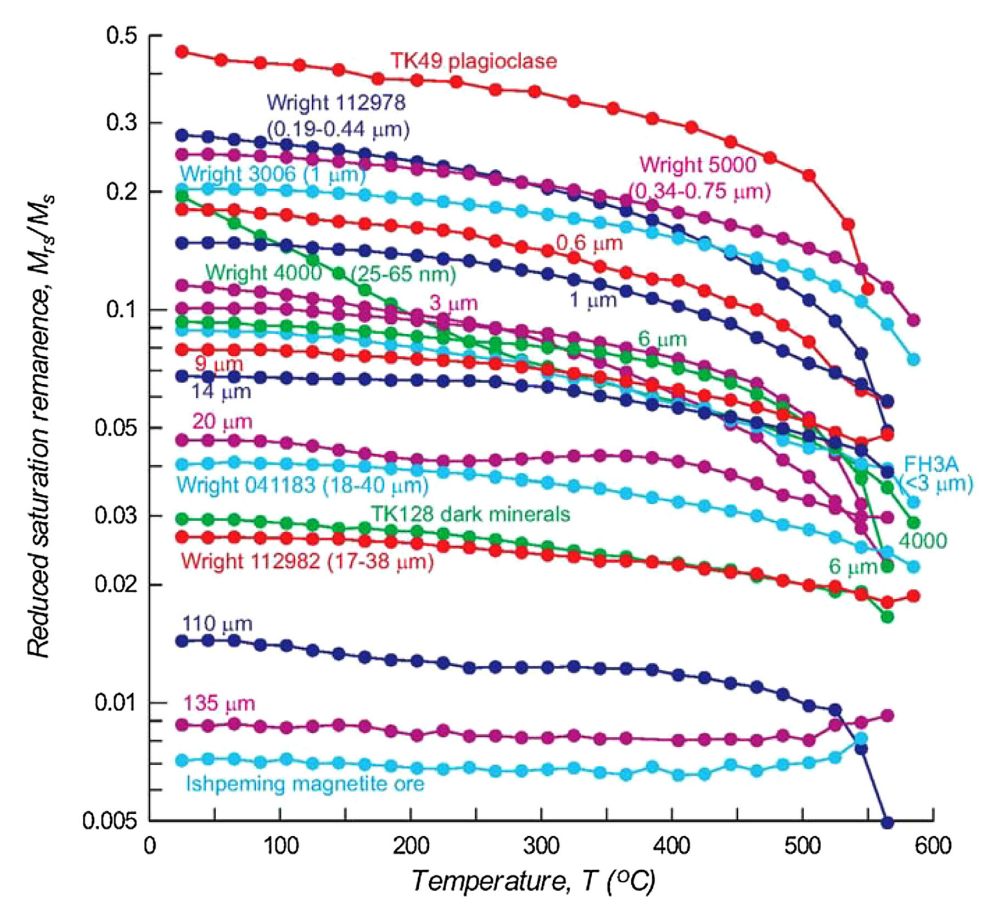


Figure 4. $M_{\rm rs}/M_{\rm s}$ versus T data for all magnetite samples plotted on a logarithmic scale. Data trends of fine-grained samples TK49 and Wright 112978 and 4000 cut across those of the other samples, probably as a result of thermal unblocking of SD grains over part or all of the T range. Samples containing large MD grains (135 μm and Ishpeming ore) have constant ratios except above 500 °C where $M_{\rm rs}/M_{\rm s}$ rises, in contrast to all other samples. Apart from aberrant 20 μm data and cross-cutting data of 3A (700 °C pre-annealed 3 μm magnetite), the remaining 13 samples have parallel trends, showing similar percentage changes, up to 450–500 °C where unblocking begins in the finer grained samples. The common pattern, over a size range spanning 0.34–0.75 μm to 110 μm, is a gentle but steady decrease in $M_{\rm rs}/M_{\rm s}$ with increasing T.

across the data trends for all other samples. Its value of $M_{\rm rs}/M_{\rm s}$ at 20 °C is only 0.195, indicating that the grain-size spectrum extends well below 25 nm and that more than half the grains are already SP at 20 °C. Grains with sizes above $d_{\rm s}$ have their coercivities reduced by thermal fluctuations (Kneller & Luborsky 1963; Dunlop & Özdemir 1997, eqn. 8.28), explaining the relatively low value of coercive force at 20 °C (16.7 mT, Table 1) and the very rapid decrease in $H_{\rm c}$ values with even the mildest heating (Fig. 5).

6 CHANGES IN H_c AND COERCIVITIES WITH TEMPERATURE

Values of coercive force H_c for all magnetite samples are plotted on a logarithmic scale as a function of T in Fig. 5. The curves are similar in general aspect to the descending $M_{\rm rs}/M_{\rm s}(T)$ curves of Fig. 4 but steeper, particularly above 500 °C. The coercive force is affected, like $M_{\rm rs}/M_{\rm s}$, by the addition of new vortices and/or domain walls to grains with heating. This must result in a re-equilibration of the micromagnetic/domain structure. For example, existing walls will move to new positions of local minimum energy. But whereas this, and actual remanence unblocking, are the sole sources of changing $M_{\rm rs}/M_{\rm s}(T)$, there are two other phenomena at play in $H_c(T)$ changes.

Independent of changing vortex/wall positions or structures, the wall and other pinning forces that control coercivity decrease with

rising temperature because of decreasing magnetoelastic and magnetocrystalline anisotropies. The resulting change in $H_c(T)$ is often described by a power-law dependence, $M_s^n(T)$. The change tends to be slow at low to intermediate T but accelerates near the Curie point. Large MD grains like those in the 135 μ m and Ishpeming samples, which maintain an unchanging domain structure almost to T_c (Fig. 4), owe their decreasing $H_c(T)$ (Fig. 5) entirely to anisotropy.

The final cause of changing $H_c(T)$ is thermal activation below the actual unblocking temperature $T_{\rm UB}$ of the grain, as described at the end of the previous section. This effect is strongest in fine grains, SD or slightly larger, and is responsible for the precipitous descent of the $H_c(T)$ curve of TK49 above ≈ 400 °C and the Wright 4000 $H_c(T)$ curves at all T (Fig. 5).

Domain structure in magnetite is often investigated using a Day plot of $M_{\rm rs}/M_{\rm s}$ versus $H_{\rm cr}/H_{\rm c}$ (Day *et al.* 1977), where $H_{\rm cr}$ is remanent coercive force. As we are dealing here with well-characterized magnetites, the objections voiced by Roberts *et al.* (2018) do not apply. However, it was decided for other reasons to forego the use of Day plots. Measuring the M-H hysteresis loop is straightforward and automated but measuring $H_{\rm cr}$, the crossover point on the reverse-field remanence curve, requires repeated H on/H off measurements and personal involvement from the experimenter to zero in on the axis-crossing field. Because of the large number of samples in this study, it was decided to save time by foregoing $H_{\rm cr}$ measurements. An alternative to the Day plot, a squareness-coercivity (SC) plot of

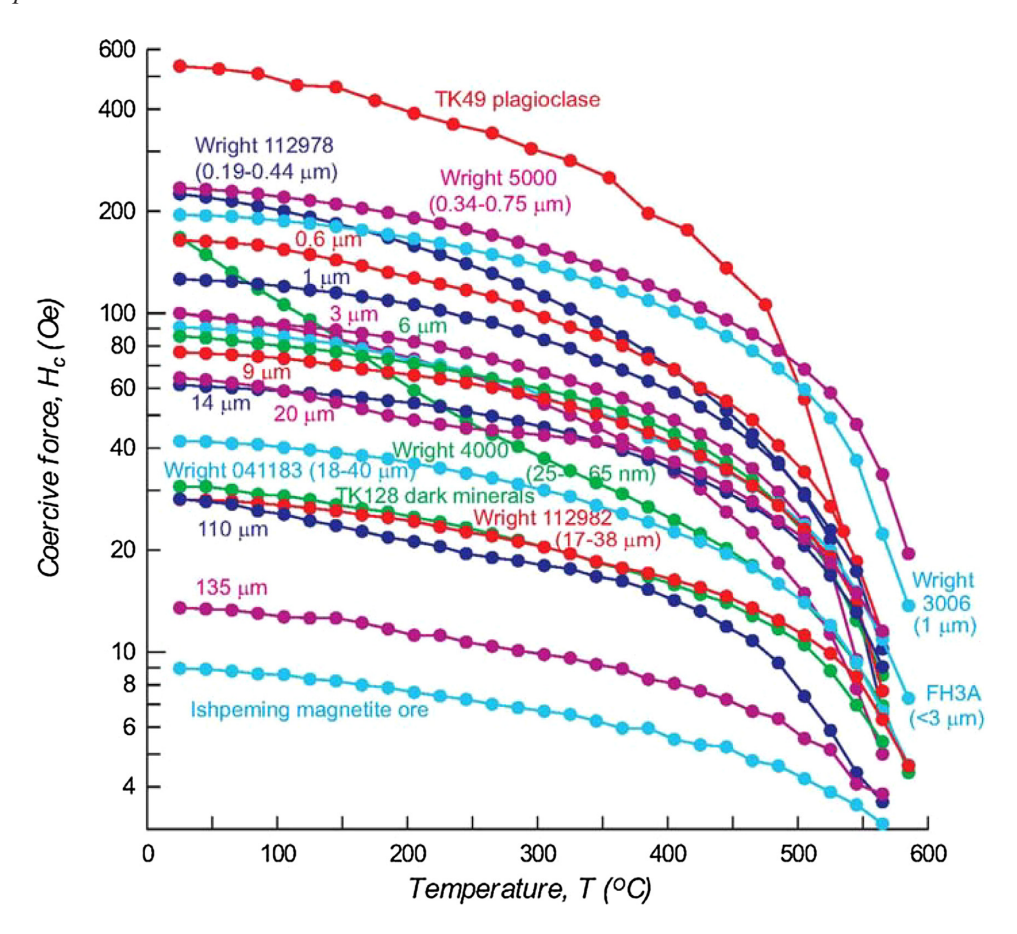


Figure 5. H_c versus T data for all magnetite samples plotted on a logarithmic scale. Apart from the more rapid decreases, the patterns are the same as in Fig. 4. TK49 and Wright 112978 and 4000 have cross-cutting trends resulting from reduction of H_c by thermal activation. The 20 μm and pre-annealed 3 μm magnetites have aberrant/cross-cutting trends. The largest MD grains (135 μm and Ishpeming ore) have gently descending $H_c(T)$ data with no sign of thermal activation even above 500 °C. The other 13 samples have subparallel $H_c(T)$ trends with steady descents and steeper plunges above 500 °C marking ultimate unblocking of all remanence carriers. Note on units: 1 Oe = 79.6 A m⁻¹; the equivalent B is 10^{-4} T.

 $M_{\rm rs}/M_{\rm s}$ versus $H_{\rm c}$ (Wasilewski 1973; Tauxe *et al.* 2002), is used to display the high-T hysteresis data in Fig. 6. $H_{\rm c}$ is not by itself diagnostic of domain structure. Hence an SC plot has no counterparts to the SP, SD, PSD or MD type curves and regions on the Day plot (Dunlop 2002a,b).

Fig. 6 separates the sample set into three parts, both for convenience of display and because each subset has its own individual behaviour. Fig. 6(a) displays data for six of the seven magnetites in the approximate size range 0.05–1 μ m. The Wright 4000 data again cut across the data trends of other samples because the fine SD material in this sample is so vulnerable to thermal activation and unblocking. The other five samples trace out a fan of similarly shaped convex-up curves, spread by about a factor 2 in both $M_{\rm rs}/M_{\rm s}$ and $H_{\rm c}$ at 25 °C and convergent at 565 °C.

Fig. 6(b) covers the classic magnetite PSD range (Stacey 1962; Parry 1965; Stacey & Banerjee 1974), displaying data for six samples in the size range 3–20 μ m. FH3A (<3 μ m) belongs in this subset because its hydrothermal origin and low internal stresses make its magnetic behaviour akin to that of stressed grains of considerably larger size; its data fall below those of the 3 μ m and 6 μ m magnetites. The FH3A data also cut across the 9 and 14 μ m data trends at high T, suggesting that FH3A contains a broad range of finer grains extending down to near-SD size which make it more vulnerable to thermal activation than the other samples. Overall the curves of five of the six samples form a nested set with less curvature

than the curves in Fig. 6(a). The data for the 20 μ m magnetite lie well below those of the other samples and seem to belong with the MD set of the next figure, apart from a peculiar interval at intermediate T in which $M_{\rm rs}/M_{\rm s}$ increases with heating (visible also in Fig. 4).

Fig. 6(c) covers the true MD range, above the breakpoint in size dependences of magnetic properties (Parry 1965; Hartstra 1982a; Dunlop 1986), and includes data for six samples with sizes, measured or inferred, ≥ 20 –40 μm . Compared to the two other subsets, these $M_{\rm rs}/M_{\rm s}$ versus $H_{\rm c}$ plots are quite linear, although they strikingly fail to approach the origin at 565 °C, only 10–20 °C below $T_{\rm C}$. The data form two separated groupings, small MD (20–40 μm) and large MD (100 μm and above). The small MD grains change domain structure more with rising T than do the large MD grains. $M_{\rm rs}/M_{\rm s}$ decreases by a factor 2 between 25 °C and 525 °C for the former group but by about half this amount for the 110 μm grains and hardly at all for the 135 μm grains and the Ishpeming ore.

7 DISCUSSION

7.1 Hematite results

Studying the high-temperature hysteresis of hematite remains a work in progress because of high coercivities, which prevent saturation in typical electromagnet fields, and contamination of

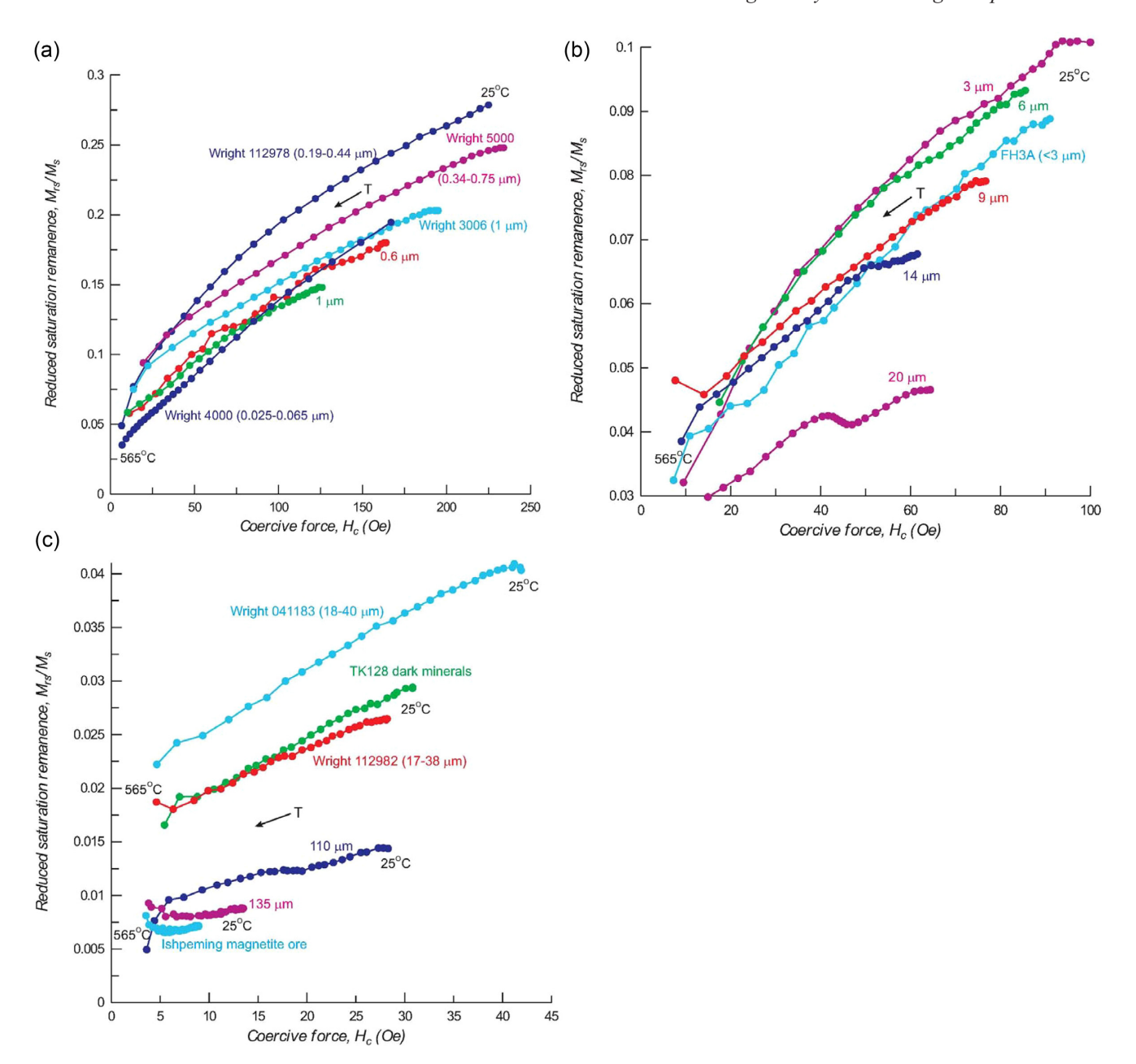


Figure 6. Temperature evolution of $M_{\rm rs}/M_{\rm s}$ and $H_{\rm c}$ data (squareness-coercivity plots). (a) Data for grain sizes ≤ 1 μm. Curves for Wright 5000, Wright 3006, 0.6 μm and 1 μm magnetites form a nested set. Wright 112978 and Wright 4000 contain thermally activated fine SD grains whose more rapidly decreasing $M_{\rm rs}/M_{\rm s}$ and $H_{\rm c}(T)$ data cut across the other trends. (b) Data for PSD sizes (3–20 μm). The 3 and 6 μm data form a set, as do the 9 and 14 μm data. Both are cross-cut by the data of FH3A, which has a broad size spectrum. The 20 μm data are clearly anomalous. (c) Data for small MD (TK128 and Wright 041183 and 112982) and large MD (110 and 135 μm and Ishpeming ore) grains. The slopes of the quasi-linear plots level out as grain size increases but in all cases $H_{\rm c}$ changes much more rapidly with T than $M_{\rm rs}/M_{\rm s}$ Note on units: 1 Oe = 79.6 A m⁻¹; the equivalent B is 10^{-4} T.

natural material by a per cent or less of magnetite. Both problems are evident in the room-temperature hysteresis loop of the Hoyt Lake sample (Fig. 1b). Only a minor loop can be measured with the peak electromagnet field of 1 T and the loop is waspwaisted. The steeply sloping section between $\pm 150\,\mathrm{mT}\,(\pm 1500\,\mathrm{Oe})$ is due mainly to magnetite, while the remaining higher-field sections, if recombined, would mimic a Rayleigh loop on a giant scale.

The (non-saturation) hysteresis parameters from higher-temperature loops (Fig. 2b) reveal the same dual effects. M_s , M_{rs} and H_c all increase in the first 10–12 heating steps and only begin to drop

above the 285 °C step, when hematite coercivities decrease enough to permit an approach to saturation. The magnetite contribution is finally eliminated above 580 °C, where $M_{\rm s}$ has an inflection point and $H_{\rm c}$ peaks.

 $M_{\rm rs}/M_{\rm s}$ is almost constant at 0.55–0.6 from 25 to 565 °C (Fig. 3). This range of values is compatible with either SD or MD hematite. However, above 580 °C, $M_{\rm rs}/M_{\rm s}$ abruptly increases to 0.7–0.72, a figure at the limit of SD values and favouring instead MD behaviour (Özdemir & Dunlop 2014). Evidently minor magnetite depresses $M_{\rm rs}/M_{\rm s}$ over the entire T range below its Curie point and may give a misleading impression of hematite grain size and domain structure.

A final intriguing observation is that $M_{\rm s}$ and $M_{\rm rs}$ both $\to 0$ in the 685 °C measurement step (Fig. 2b) but $H_{\rm c}$ retains 15 per cent of its initial value above the nominal 675 °C hematite Curie point. At the same temperature, $M_{\rm rs}/M_{\rm s}$ still has about $\frac{1}{2}$ its peak value (Fig. 3), although $M_{\rm s}$ and $M_{\rm rs}$ are both so small at 685 °C that the exact value of $M_{\rm rs}/M_{\rm s}$ is debatable.

7.2 Pyrrhotite results

Pyrrhotite (Fe_{1-x}S, $x \le 0.125$) owes its magnetism to the preferential location of Fe2+ vacancies on alternate cation basal planes (Bertaut 1953; Schwarz & Vaughan 1972; Powell et al. 2004; see also Dunlop & Özdemir 1997, fig. 3.26). The vacancy ordering is expressed in terms of the stacking modulation, the repeat distance between identical Fe²⁺ layers in the hexagonal NiAs structure of alternating Fe and S planes. Only the most cation-deficient end member, with a monoclinic 4C vacancy superstructure (4th layer repeat), is fully ordered and stably ferrrimagnetic over the entire range from 0 K to the Curie point $T_{\rm C} = 325 \,^{\circ}{\rm C} \, (\approx 600 \, {\rm K})$. Its ideal chemical formula is Fe₇S₈, although small admixtures of sulphides with other compositions and vacancy superstructures may change this slightly (e.g. Charilaou et al. 2015). Exchange coupling of Fe²⁺ ions is ferromagnetic within c-planes, with a comparatively strong triaxial anisotropy (Bin & Pauthenet 1963); interlayer coupling is antiferromagnetic.

The approach to the Curie temperature is marked by cation diffusion between vacancy sites, either direct or via one or more tetrahedral interstices in the lattice. Interlayer diffusion has the shortest and most direct path (Koulialias *et al.* 2019b, fig. 7) and dominates. It decreases the vacancy ordering, since each jump replaces a vacancy by an Fe²⁺ ion, and thus reduces the ferrimagnetic moment. At $T_{\rm C}$ the ferrimagnetism disappears, not because of the breakdown of exchange coupling and the onset of paramagnetism as in most ferrimagnets but because the 1C random vacancy ordering superstructure above $T_{\rm C}$ yields no net moment.

Finding a pure 4C pyrrhotite sample proved difficult. Natural pyrrhotites often are a mixture of cation-deficient iron sulphides, of which Fe₉S₁₀ in particular is ferrimagnetic between 200 and 265 °C (Schwarz 1975; Dunlop & Özdemir 1997, fig. 3.27). Pyrrhotites also often contain magnetite and many additionally develop magnetite through oxidation in the course of heating. Unlike the situation with hematite, magnetite and pyrrhotite have $M_{\rm s}$ values that are not grossly dissimilar (480 and \approx 80 kA m⁻¹, respectively) with the result that a minor amount of magnetite will not swamp pyrrhotite's magnetic signal. However, whereas hematite has a higher $T_{\rm C}$ and orders-of-magnitude higher coercivities than magnetite, making the magnetic signals of the two minerals easy to recognize and separate, pyrrhotite has a lower $T_{\rm C}$ than magnetite and fairly similar coercivities. A superimposed magnetite signal cannot readily be recognized in hysteresis or separated by heating.

The Santa Eulalia pyrrhotite has SD behaviour at 20 °C (Fig. 1a) but upon heating $M_{\rm rs}$ decreases more rapidly than $M_{\rm s}$ from the very first temperature steps (Fig. 2a). $M_{\rm rs}/M_{\rm s}$ drops below 0.5 by 200 °C and reaches 0.21 at 305 °C (Fig. 3). The most obvious explanation for this rapid decrease, particularly between 225 and 305 °C, is thermal unblocking of SD grains. The SP threshold size $d_{\rm s}$ for pyrrhotite can be estimated by equating the energy barrier $\frac{1}{2}\mu_0VM_{\rm s}H_{\rm c}$ to the available thermal energy 25kT (cf. Dunlop & Özdemir 1997, eq. 5.29), which yields $d_{\rm s}\approx 0.046~\mu{\rm m}$ at room temperature. With increasing T, the thermal energy 25kT grows while the energy barrier to rotation of SD moments shrinks, with

the result that d_s increases, eventually sweeping through the entire size distribution of the sample as $T \rightarrow T_C$.

Another possible explanation for the strong decreases in $M_{\rm rs}/M_{\rm s}$ with heating is a change of domain structure from SD to another thermally stable but less potently magnetic state. The first such change to occur with an increase of grain size d at constant T is the flower state but because it involves only a rotation of corner spins the reduction in grain moment is minor. More significant is twisting of the entire spin structure in the vortex state, which reduces the magnetic moment to levels almost as low as thermal unblocking. Whether or not these changes are likely to occur when T increases for a grain of fixed size d is unclear. In magnetite, the critical size d_0 for the nucleation of incoherent structures in SD grains is thought to remain relatively constant with heating rather than decreasing (see next section).

A third possible cause of decreasing $M_{\rm rs}/M_{\rm s}$, particularly in the $100\,^{\circ}{\rm C}$ or so below $T_{\rm C}$, is cation migration from Fe-rich to Fe-poor c-planes, reducing the vacancy ordering and with it the ferrimagnetic moment (Koulialias et~al.~2019b). Furthermore, cation diffusion may not be uniform. The Santa Eulalia pyrrhotite is polycrystalline, and even individual crystals may well be subdivided into separate 4C regions, as detected by X-ray diffraction (Koulialias et~al.~2019a). Conceivably these microstructural effects could favour the formation of vortices or domain-wall nuclei (half-vortices), indirectly influencing the magnetism.

 $H_{\rm c}$, like $M_{\rm rs}$, decreases more rapidly with heating than $M_{\rm s}$ (Fig. 2a). The two change in almost identical ways up to the 150 °C step, after which $H_{\rm c}$ drops more quickly. This is as expected for thermal activation. $H_{\rm c}$ should decrease faster with increasing T than $M_{\rm rs}$ because thermal unblocking of remanence occurs only at the grain's unblocking temperature $T_{\rm UB}$ but coercive force is reduced by thermal fluctuations well below $T_{\rm UB}$ (Dunlop & Özdemir 1997, eqn. 8.24).

In the final heating step, H_c changes trend and does not approach zero like $M_{\rm rs}$ and $M_{\rm s}$ The same behaviour is seen for the Hoyt Lake hematite (Fig. 2b) and for some but not all magnetites, for example, cf. TK49 and TK128 (Figs 2c and d). Some of the H_c residuals at the nominal Curie temperatures of the various minerals are sizeable and do not seem to be explicable as a quirk in the MicroVSM software. If the H_c residuals are in fact real, they would have to be due to a small amount of some mineral with a higher Curie point, likely magnetite in the case of the Santa Eulalia pyrrhotite and hematite for those magnetites that show residuals.

7.3 Magnetite results

Of the two SD magnetites in this study, TK49 contains only a little SP material at room temperature T_0 , as evidenced by its 20 °C $M_{\rm rs}/M_{\rm s}$ value of 0.455, while Wright 4000 has an $M_{\rm rs}/M_{\rm s}$ value of 0.195 and must contain a major SP fraction at T_0 . Both samples have properties that suggest thermal activation (Figs 2c, 4 and 5.) $M_{\rm rs}(T)$ and $H_{\rm c}(T)$ fall rapidly (quasi-linearly for TK49) relative to $M_{\rm s}(T)$ over the entire range from T_0 to $T_{\rm C}$ and T_0 falls more rapidly than T_0 that T_0 is econd property follows from the fact that grains which are still below $T_{\rm UB}$ and do not yet contribute to the decrease in T_0 have already had their T_0 reduced by thermal activation.

 $M_{\rm rs}/M_{\rm s}$ and $H_{\rm c}$ were plotted on logarithmic scales in Figs 4 and 5. One important result of this method of plotting is that equal increments at any level of the ordinate represent equal percentage changes in $M_{\rm rs}/M_{\rm s}$ or $H_{\rm c}$. It is striking to the eye that almost all

the samples have similarly shaped $M_{\rm rs}(T)/M_{\rm s}(T)$ graphs and likewise similar $H_{\rm c}(T)$ graphs. Exceptions are the finest grained samples, TK49, Wright 4000 and 112978 (which seems to contain grains much smaller than its nominal size range of 0.19–0.44 µm); the 20 µm magnetite, with anomalous increases in $M_{\rm rs}/M_{\rm s}$ above 300 °C; and the large MD samples 135 µm and Ishpeming, for which $M_{\rm rs}/M_{\rm s}$ is almost constant with T while $H_{\rm c}$ decreases more gradually than for the other samples.

The central set of graphs with similar T dependences of $M_{\rm rs}/M_{\rm s}$ and of $H_{\rm c}$ includes samples spanning the broad size range from $\approx 0.5~\mu {\rm m}$ (Wright 5000, $0.6~\mu {\rm m}$) through the PSD range (FH3A, 1, 3, 6, 9 and 14 $\mu {\rm m}$) into small to moderate MD sizes (TK128, Wright 041183 and 112982, 110 $\mu {\rm m}$). Taken individually, these samples have another feature in common, namely $M_{\rm rs}(T)$ and $H_{\rm c}(T)$ dependences that are nearly identical to each other, in contrast to thermally activated SD grains where $H_{\rm c}(T)$ decreases more rapidly than $M_{\rm rs}(T)$.

The similarity of temperature dependences of $M_{\rm rs}/M_{\rm s}$ over such a broad size range is intriguing. In each case $M_{\rm rs}/M_{\rm s}$ decreases continuously from T_0 to T_C in an entirely different way from the thermal activation decreases of TK49 and especially Wright 4000 (Fig. 4). The same is true for the $H_c(T)$ dependences in Fig. 5, where the cross-cutting trends of TK49 and 4000 are even more obvious. Some process or processes other than thermal activation must be at work in these intermediate-size magnetites. Non-thermally activated changes towards states with lower capacity for carrying remanence might include the development of vortices or partial vortices (twisting of spins at opposite sides of a grain to form a domain-wall nucleus) in SD grains, reversion of metastable SD grains to lowerremanence LEM (local energy minimum) states, nucleation of new domains via reverse spikes at domain edges and interior cracks, and re-equilibration of existing walls due to decreasing wall-pinning energy with increasing T.

Almeida et al. (2016) have made direct high-temperature observations using off-axis electron holography of the magnetic vortex structure and thermal demagnetization of a 250 nm octahedral magnetite crystal. The basic vortex pattern remains almost unchanged until 500 °C and on cooling to 20 °C from temperatures as high as 600 °C, the original vortex structure or its mirror image are recovered. The initial remanence, due to a vortex core revealed by micromagnetic calculations, decreases very slowly until above 540 °C, where it drops rapidly in the manner of unblocking of SD structures at similar temperatures. Thus thermally driven unpinning of a stable vortex structure cannot be the source of the similar T dependences of $M_{\rm rs}/M_{\rm s}$ and of $H_{\rm c}$ seen in Figs 4 and 5 from ≈ 500 nm through the entire PSD size range. On the other hand, although 250 nm magnetites may not nucleate further vortices in the course of heating, larger grains could possibly do so and thus give rise to remanence (and coercivity) decreases at intermediate T.

Despite recent assertions (Roberts *et al.* 2017), except for $< 1~\mu m$ sizes just above d_0 , vortices alone cannot be at the heart of the PSD phenomenon—the continuous and gradual rather than abrupt decrease from SD values of remanence and coercivity with increasing grain size. Three to five body domains are seen by magnetic force microscopy in 5 μm to 13 μm magnetite crystals (Pan *et al.* 2002) and domain multiplicities from two to as high as ten $(0.5-20~\mu m$ grains) are revealed by Bitter patterns and other imaging methods (summary in Özdemir & Dunlop 2006, figs. 13 and 14, and Dunlop & Özdemir 2015, fig. 7). In many cases, there are fewer body domains than predicted by equilibrium domain theory, either because of stabilizing closure domains or because the grains are in metastable high-remanence LEM states, but there is

no question that well-developed domains and walls are the norm throughout most of the magnetite grain size range from 1 to 20 μm.

Few theoretical/empirical estimates have been made of temperature driven domain structure changes. Dunlop (1987, fig. 9) made three independent estimates of the T dependence of the SD threshold size d_0 using $M_{\rm rs}/M_{\rm s}$ and $H_{\rm c}$ data in concert with theoretical predictions, for example, those of Halgedahl & Fuller (1983). In all cases, d_0 remained essentially constant or increased slightly with rising T. Close to $T_{\rm C}$, d_0 rose sharply; this is logical because wall-pinning energies, whether magnetocrystalline, magnetoelastic or magnetostatic in origin, all decrease with increasing T as a power of $M_{\rm s}(T)$ while the driving energy due to an applied field H_0 decreases as $M_{\rm s}(T)$. Near $T_{\rm C}$, even a small field will drive out domain walls and saturate a grain.

Calculations that take account of the coexistence of SD and other competing LEM states of lower net moment (most convincingly demonstrated experimentally for pyrrhotite and high-Ti titanomagnetite) give similar results. The size range over which SD and two-domain states are theoretically both possible in magnetite narrows with rising T, and above 500 °C both d_0 and $d_{\rm SD}^{\rm max}$ rise (Dunlop *et al.* 1994; Dunlop & Özdemir 1997, fig. 5.15). These calculations may not be very realistic, however, given that the transformation from SD to 2-domain at constant T and changing d is indirect, via intermediate flower and vortex states.

The major theoretical study of equilibrium numbers and sizes of domains with heating (Moskowitz & Halgedahl 1987) is for TM60 (titanomagnetite with 60 mol per cent Ti), not magnetite. A variety of power-law dependences of exchange and magnetostriction constants on $M_s(T)$ were tried with model grain sizes ranging from 0.2 to 25 μ m. For almost all models the number of domains increased with rising T. In a 2- μ m grain containing 2 domains at 25 °C, the equilibrium number of domains increased to 3 in the course of mild heating for four models, and ultimately to 6 and 9 in two other models. Wall widths, which are proportional to $(A/K)^{1/2}$ (A and K are exchange and magnetocrystalline anisotropy constants), increased substantially with heating because K decreases as a higher power of $M_s(T)$ than A. This is a property of ferromagnetic minerals generally and could lead to unpinning of walls at high T.

Experimental observations of domains in magnetite at elevated temperatures are as sparse as theoretical studies. Bitter patterns observed by Heider $\it et~al.~(1988)$ on euhedral magnetite crystals became obscure by 350 °C because of wall broadening. Most large ($\geq 30~\mu m)$ crystals exhibited some rearrangement of domain patterns with heating to only 120 °C as well as edge nucleation of spike domains which in some cases expanded to form new body domains. A fraction of small ($\leq 10~\mu m)$ crystals had simple structures, such as two body domains + closure domain(s), which did not change with heating. The domain structure after a heating-cooling cycle was variable, resembling but not duplicating the original pattern, and containing from two to five body domains in repeated cycling.

The only other study on magnetite, by Ambatiello *et al.* (1999), used the magneto-optical Kerr effect, which images entire domains through the rotation of the plane of polarization of light by surface magnetization. In this way domains could be resolved up to $550\,^{\circ}\mathrm{C}$ on the polished surface of a mm-size magnetite crystal. Up to $400\,^{\circ}\mathrm{C}$, there were only minor changes in widths of lamellar body domains. Above $400\,^{\circ}\mathrm{C}$, domains increased in width on heating and shrank reversibly on cooling without any striking changes in pattern.

Neither of these studies involved observing domain structures in the course of a hysteresis cycle. Metastable LEM states different from the equilibrium or GEM (global energy minimum) state are more frequent in saturation remanence after field cycling than after weak- or zero-field temperature cycling to the Curie point (Halgedahl & Fuller 1983; Boyd *et al.* 1984; Metcalf & Fuller 1987; Halgedahl 1991). Usually these states have higher magnetic moments than the GEM state. They may play a role in the $M_{\rm rs}/M_{\rm s}$ results of Fig. 4 that would not be obvious from experimental or theoretical studies of domains in low-field thermal cycling. It is also well known that LEM states of high moment, e.g. metastable SD states, often nucleate domains in small reverse fields (Halgedahl & Fuller 1983). Thus the magnetic state of a grain at saturation remanence (Fig. 4) is potentially different from that at a reverse field $-H_{\rm c}$ (Fig. 5).

That said, the predictions and observations of domain styles and numbers at high temperature in magnetite do not offer much encouragement in interpreting the gentle but continuous drop in $M_{\rm rs}/M_{\rm s}$ values over the entire T_0 to $T_{\rm C}$ range for almost all the samples in Fig. 4 (see also Yu *et al.* 2004, fig. 3). The same pattern of gradual decrease in $M_{\rm rs}/M_{\rm s}$ values with heating appears in elongated SD grains and in equant grains with sizes at and above d_0 (76, 100 and 220 nm; Dunlop 1987, fig. 4), which begin to unblock only above 550 °C (Dunlop 1976, fig. 2). The high $T_{\rm UB}$ values are due either to grain elongation or, for the equant grains, narrow size spectra that end well above the SP threshold $d_{\rm s}$. They do not have the thermal activation characteristics outlined at the beginning of this section but instead behave like grains in the PSD range.

The only remaining mechanism for decreasing $M_{\rm rs}/M_{\rm s}$ values in hysteresis cycles at higher T is re-equilibration of either vortex patterns (see, however, Almeida et~al.~2016) or domain wall positions. This could be temperature-driven, resulting purely from changes in crystalline and magnetoelastic pinning energies between T steps, field-driven in the course of hysteresis, or a result of nucleating new vortices or domains, e.g. as LEM states approach the GEM state. However, the largest magnetite grains, Ishpeming and 135 μ m, which contain the most walls for re-equilibration, have almost unchanging $M_{\rm rs}/M_{\rm s}$ values from T_0 to 500 °C (Fig. 4) and the gentlest descent in $H_{\rm c}$ values above 400 °C (Fig. 5).

Whatever its cause, the fact that M_{rs}/M_s values typically decrease at elevated temperatures has potential implications for TRM acquisition because the inverse effect should be an increase in remanence carrying capacity upon cooling. The present data are based on changing magnetic field H at constant temperature T but changing T at constant H may well access a similar succession of states, despite the very different field strengths involved in hysteresis measurements and TRM. Domain-wall configurations that re-equilibrated during heating might be at least partially reincarnated during cooling, as domains denucleate to create LEM states with fewer domains and higher moments. Major increases in remanence capacity would result from a transformation from vortex to stable SD structure in the course of cooling, or in larger grains, transformation from 2-domain to a metastable SD state. The observations and theories of kinematic TRM acquisition in MD and PSD magnetite by Sugiura (1981, 1988), McClelland & Sugiura (1987) and McClelland & Shcherbakov (1995) lend some support to these speculations.

Combining the $M_{\rm rs}/M_{\rm s}$ and $H_{\rm c}$ data of individual samples in the squareness-coercivity (SC) plots of Fig. 6 adds no new information but does make related and discrepant trends easier to recognize. In Fig. 6a, Wright 5000 and 3006 plus the 0.6 and 1 μ m magnetites form a group with parallel trends. Plots for the thermally activated magnetites Wright 4000 and 112978 cut across these trends. In Fig. 6(b), apart from the wildcat 20 μ m sample, the 3 and 6 μ m magnetites form a set, the 9 and 14 μ m magnetites a second set, while the cross-cutting FH3A data share some attributes of each.

Size distribution—broadest for FH3A—is the cogent factor here. In Fig. 6(c), Wright 041183 and 112982 form a group with the TK128 dark minerals, placing its magnetite grain sizes in the 20–40 μ m range. The Ishpeming and 135 μ m magnetites data resemble each other, while the 110 μ m magnetite belongs more with the 20–40 μ m trends. These associations of trends are useful hints but it would not be possible to say much about the mechanisms of high-temperature $M_{\rm Ts}/M_{\rm S}$ and $H_{\rm C}$ behaviour on the basis of SC plots alone.

8 CONCLUSIONS

The hysteresis data in this study were measured at 10 or 20 °C intervals from 25 °C to the Curie temperature for one hematite sample (with slight magnetite contamination), one SD pyrrhotite sample, and 20 magnetite samples with room-temperature domain states ranging from SP/SD to large MD. The reported hysteresis parameters $M_{\rm s}$, $M_{\rm rs}$, $M_{\rm rs}$ / $M_{\rm s}$ and $H_{\rm c}$ are values at or following technical saturation, except for the hematite sample below \approx 300 °C. The resolution of these measurements is greater than that in any previous study in terms of spacing of temperature steps and coverage of magnetite grain sizes and domain structures.

Hematite and magnetite signals are superimposed in the Hoyt Lake data. Above magnetite's Curie point, M_{rs}/M_s is ≥ 0.7 , compatible with either SD or MD structure. However, the high coercivities, some > 1 T, imply SD crystallite sizes.

The Santa Eulalia 4C monoclinic pyrrhotite has SD behaviour at room temperature ($M_{\rm rs}/M_{\rm s}=0.575$) but $M_{\rm rs}/M_{\rm s}$ decreases to 0.2 in measurements at 300 °C. $M_{\rm rs}(T)$ and $H_{\rm c}(T)$ drop rapidly compared to $M_{\rm s}(T)$ from 25 to 325 °C, $H_{\rm c}(T)$ more quickly than $M_{\rm rs}(T)$. These magnetic changes may be due in part to cation migration between vacancy-poor and vacancy-rich Fe layers.

Two submicron synthetic magnetites and one natural sample (TK49: SD magnetite inclusions in plagioclase) contain significant SP size fractions at 25 °C. Their rapid $M_{\rm rs}(T)$ and $H_{\rm c}(T)$ decreases at higher T indicate thermal remanence unblocking (SD \rightarrow SP) and thermal activation below $T_{\rm UB}$, and are not due to SD grains nucleating vortices or domain walls.

Two samples containing the largest magnetite grains (135 μ m and Ishpeming ore) have $M_{\rm rs}/M_{\rm s}$ values that do not change appreciably with T except in the final few steps, as well as gently descending $H_{\rm c}(T)$ values. Their MD structures remain unchanged with heating except for minor wall displacements facilitated by decreasing wall pinning. Thermal fluctuations cause unblocking only very close to $T_{\rm C}$.

All other magnetites, spanning sizes from 0.5 to 110 µm, have a common behaviour which is distinct from that of the thermally activated SD grains or the M_{rs}/M_s invariant MD grains. M_{rs}/M_s decreases continuously but gradually as T increases, then more rapidly above 500 °C. In addition, $M_{rs}(T)$ and $H_c(T)$ decreases are almost identical. The same behaviour is observed for SD and slightly larger than SD grains that lack room-temperature SP fractions and only unblock above 550 °C (Dunlop 1987), as well as for some annealed PSD-size magnetites (Yu et al. 2004, figs 2, 3). Many mechanisms could account for the near-universal decrease of $M_{\rm rs}/M_{\rm s}$ with increasing T: nucleation of vortices in SD grains; nucleation of domains that reduce high-remanence LEM states towards GEM states; and major wall motions, including those due to re-equilibration of the domain structure resulting from LEM transitions. Domain observations offer some support for the latter two mechanisms but most observed domain nucleations and major wall motions occurred below 150 °C (Heider et al. 1988; Heider 1990).

Since remanence carrying capacity, as measured by $M_{\rm rs}/M_{\rm s}$, typically decreases with heating, logically remanence states of higher magnetic moment should become available in the course of cooling. The general tendency would be for grains to denucleate domains and/or vortices as they cool, perhaps remobilizing domain walls in the process. Although speculative, this scenario has some support in observations (Heider *et al.* 1988) and ideas about kinematic TRM acquisition in MD and PSD magnetite (e.g. McClelland & Sugiura 1987)

In some but not all samples, $M_{\rm rs}$ and $M_{\rm s}$ drop smoothly to zero at high T but $H_{\rm c}$ retains a non-zero value at the nominal $T_{\rm C}$. If not an artefact of the data analysis software, the $H_{\rm c}$ residuals may indicate trace amounts of a mineral with a higher $T_{\rm C}$.

ACKNOWLEDGEMENTS

The measurements were carried out during several periods as a visiting fellow at the Institute of Rock Magnetism, which operates with support from the National Science Foundation, Earth Sciences Division and the University of Minnesota. Thanks to Subir Banerjee and Bruce Moskowitz for hosting the visits and to Mike Jackson and Peat Sølheid for discussions and help with the instruments and programs. Franz Heider, Özden Özdemir and Joseph Hodych provided samples; Song Xu separated size fractions and characterized the crushed magnetites. In-depth comments and suggestions by Mark Dekkers and Andreas Gehring were much appreciated. This research was supported by the Natural Sciences and Engineering Research Council of Canada. Data reported in this paper are available from the author on request.

REFERENCES

- Almeida, T.P., Kasama, T., Muxworthy, A.R., Williams, W., Nagy, L. & Dunin-Borkowski, R.E., 2014. Observing thermomagnetic stability of nonideal magnetite particles: good paleomagnetic recorders? *Geophys. Res. Lett.*, 41, 7041–7047.
- Almeida, T.P. et al., 2016. Direct observation of the thermal demagnetization of magnetic vortex structures in nonideal magnetite recorders, *Geophys. Res. Lett.*, **43**, 8426–8434.
- Ambatiello, A., Fabian, K. & Hoffmann, V., 1999. Magnetic domain structure of multidomain magnetite as a function of temperature: observations by Kerr microscopy, *Phys. Earth planet. Inter.*, **112**, 55–80.
- Argyle, K. & Dunlop, D.J., 1990. Low-temperature and high-temperature hysteresis of small multidomain magnetites (215–540 nm), *J. geophys. Res.*, 95, 7083–7096.
- Banerjee, S.K., 1971. New grain size limits for palaeomagnetic stability in haematite, *Nat. Phys. Sci.*, **232**, 15–16.
- Berndt, T.A. & Chang, L., 2018. Theory of stable multi-domain thermoviscous remanence based on repeated domain-wall jumps, *J. geophys. Res.*, **123**, 2018JB016816, doi:10.1029/2018JB016816.
- Bertaut, E.F., 1953. Contribution à l'étude des structures lacunaires, *Acta Cryst.*, **6**, 557–561.
- Bin, M. & Pauthenet, R., 1963. Magnetic anisotropy in pyrrhotite, *J. appl. Phys.*, **34**, 1161–1162.
- Bina, M.-M. & Prévot, M., 1989. Thermomagnetic investigation of titanomagnetite in submarine basalts: eidence for differential maghemitization, *Phys. Earth planet. Inter.*, 54, 169–179.
- Boyd, J.R., Fuller, M. & Halgedahl, S.L., 1984. Domain wall nucleation as a controlling factor in the behavior of fine magnetic particles in rocks, *Geophys. Res. Lett.*, **11**, 193–196.
- Carter-Stiglitz, B., Moskowitz, B., Solheid, P., Berquó, T.S., Jackson, M. & Kosterov, A., 2006. Low-temperature magnetic behavior of multidomain titanomagnetites: TM0, TM16, and TM35, J. geophys. Res., 111, B12S05, doi:10.1029/2006JB004561.

- Charilaou, M., Kind, J., Koulialias, D., Weidler, P.G., Mensing, C., Löffler, J.F. & Gehring, A.U., 2015. Magneto-electronic coupling in modulated defect-structures of natural Fe_{1-x}S, *J. appl. Phys.*, 118, 083903, doi:10.1063/1.4929634.
- Chevallier, R. & Mathieu, S., 1943. Propriétés magnétiques des poudres d'hématite; Influence des dimensions des grains, *Ann. Phys.*, 18, 258– 288.
- Clark, D.A., 1984. Hysteresis properties of sized dispersed monoclinic pyrrhotite grains, *Geophys. Res. Lett.*, **11**, 173–176.
- Day, R., Fuller, M. & Schmidt, V.A., 1977. Hysteresis properties of titanomagnetites: grain-size and compositional dependence, *Phys. Earth planet. Inter.*, 13, 260–267.
- de Boer, C.B. & Dekkers, M.J., 1998. Thermomagnetic behavior of haematite and goethite as a function of grain size in various non-saturating magnetic fields, *Geophys. J. Int.*, **133**, 541–552.
- Dekkers, M.J., 1988. Magnetic properties of natural pyrrhotite Part I: behaviour of initial susceptibility and saturation-magnetization-related rockmagnetic parameters in a grain-size dependent framework, *Phys. Earth planet. Inter.*, **52**, 376–393.
- Dekkers, M.J. & Linssen, J.H., 1989. Rockmagnetic properties of fine-grained natural low-temperature haematite with reference to remanence acquisition mechanisms in red beds, *Geophys. J. Int.*, 99, 1–18.
- Dunlop, D.J., 1973. Superparamagnetic and single-domain threshold sizes in magnetite, *J. geophys. Res.*, 78, 1780–1793.
- Dunlop, D.J., 1976. Thermal fluctuation analysis: a new technique in rock magnetism, J. geophys. Res., 81, 3511–3517.
- Dunlop, D.J., 1986. Hysteresis properties of magnetite and their dependence on particle size: a test of pseudo-single-domain remanence models, *J. geophys. Res.*, 91, 9569–9584.
- Dunlop, D.J., 1987. Temperature dependence of hysteresis in 0.04–0.22 μm magnetites and implications for domain structure, *Phys. Earth planet. Inter.*. 46, 100–119.
- Dunlop, D.J., 2002a. Theory and application of the Day plot (M_{TS}/M_S) vs H_{CT}/H_C), 1. Theoretical curves and tests using titanomagnetite data, *J. geophys. Res.*, **107**(B3), 2056, doi:10.1029/2001JB000486.
- Dunlop, D.J., 2002b. Theory and application of the Day plot $(M_{\rm rs}/M_{\rm s} \ {\rm vs}\ H_{\rm cr}/H_{\rm c})$, 2. Application to data for rocks, sediments and soils, *J. geophys. Res.*, **107**(B3), 2057, doi:10.1029/2001JB000487
- Dunlop, D.J. & Bina, M-M., 1977. The coercive force spectrum of magnetite at high temperatures: evidence for thermal activation below the blocking temperature, *Geophys. J. R. astr. Soc.*, **51**, 121–147
- Dunlop, D.J. & Özdemir, Ö., 1997. Rock Magnetism: Fundamentals and Frontiers: Cambridge Studies in Magnetism, Vol. 3, 573pp., Cambridge Univ Press
- Dunlop, D.J. & Özdemir, Ö., 2015. Magnetizations in rocks and minerals, in *Treatise on Geophysics, Vol. 5 Geomagnetism*, 2nd edn, pp. 255–308, ed. Schubert, G., Elsevier.
- Dunlop, D.J. & Xu, S., 1994. Theory of partial thermoremanent magnetization in multidomain grains, 1. Repeated identical barriers to wall motion (single microcoercivity), *J. geophys. Res.*, 99, 9005–9023.
- Dunlop, D.J., Newell, A.J. & Enkin, R.J., 1994. Transdomain thermoremanent magnetization, *J. geophys. Res.*, 99, 19741–19755.
- Dunlop, D.J., Özdemir, Ö. & Xu, S., 2018. Magnetic hysteresis of 0.6– 110 μm magnetites across the Verwey transition, Can. J. Earth Sci., 56, 958–972.
- Dunlop, D.J., Zhang, B. & Özdemir, Ö., 2005. Linear and non-linear Thellier paleointensity behavior of natural minerals, *J. geophys. Res.*, 110, B01103, doi: 10.1029/2004JB003095.
- Eaton, J.A. & Morrish, A.H., 1969. Magnetic domains in hematite at and above the Morin transition, *J. appl. Phys.*, **40**, 3180–3185.
- Everitt, C.W.F., 1962. Thermoremanent magnetization, III. Theory of multidomain grains, *Phil. Mag.*, 7, 599–616.
- Halgedahl, S.L., 1991. Magnetic domain patterns observed on synthetic Ti-rich titanomagnetite as a function of temperature and in states of thermoremanent magnetization, *J. geophys. Res.*, 96, 3943–3972.

- Halgedahl, S.L. & Fuller, M., 1983. The dependence of magnetic domain structure upon magnetization state with emphasis on nucleation as a mechanism for pseudo-single-domain behavior, *J. geophys. Res.*, **88**, 6505–6522
- Harrison, R.J., Dunin-Borkowski, R.E. & Putnis, A., 2002. Direct imaging of nanoscale magnetic interactions in minerals, *Proc. Natl. Acad. Sci.* USA, 99, 16556–16561.
- Hartstra, R.L., 1982a. Grain-size dependence of initial susceptibility and saturation magnetization related parameters of four natural magnetites in the PSD-MD range, *Geophys. J. R. astr. Soc.*, 71, 477–495.
- Hartstra, R.L., 1982b. A comparative study of the ARM and Irs of some natural magnetites of MD and PSD grain size, *Geophys. J. R. astr. Soc.*, 71, 497–518.
- Heider, F., 1990. Temperature dependence of domain structure in natural magnetite and its significance for multi-domain TRM models, *Phys. Earth* planet. Inter., 65, 54–61.
- Heider, F., Dunlop, D.J. & Sugiura, N., 1987. Magnetic properties of hydrothermally recrystallized magnetite crystals. Science, 236, 1287–1290.
- Heider, F., Halgedahl, S.L. & Dunlop, D.J., 1988. Temperature dependence of magnetic domains in magnetite crystals, *Geophys. Res. Lett.*, 15, 499– 502.
- Jackson, M., Worm, H-U. & Banerjee, S.K., 1990. Fourier analysis of digital hysteresis data: rock magnetic applications, *Phys. Earth planet. Inter.*, 65, 78–87.
- Keller, R. & Schmidbauer, E., 1999. Magnetic hysteresis properties and rotational hysteresis losses of synthetic stress-controlled titanomagnetite particles: 1. Magnetic hysteresis properties, *Geophys. J. Int.*, 138, 319– 333.
- Kletetschka, G. & Wasilewski, P.J., 2002. Grain size limit for SD hematite, Phys. Earth planet. Inter., 129, 173–179.
- Kneller, E.F. & Luborsky, F.E., 1963. Particle size dependence of coercivity and remanence of single-domain particles, *J. appl. Phys.*, 34, 656–658.
- Koulialias, D., Lesniak, B., Schwotzer, M., Weidler, P.G., Löffler, J.F. & Gehring, A.U., 2019a. The Besnus transition in single-domain 4C pyrrhotite, *Geochem. Geophys. Geosyst.*, 20, 5216–5224.
- Koulialias, D., Weidler, P.G., Charilaou, M., Löffler, J.F. & Gehring, A.U., 2019b. Cation diffusion patterns across the magneto-structural transition in Fe₇S₈, Phys. Chem. Chem. Phys., 21, 13 040–13 046.
- Levi, S. & Merrill, R.T., 1978. Properties of single-domain, pseudo-single-domain and multidomain magnetite, J. geophys. Res., 83, 309–323.
- McClelland, E. & Shcherbakov, V.P., 1995. Metastability of domain state in multidomain magnetite: consequences for remanence acquisition, J. geophys. Res., 100, 3841–3857.
- McClelland, E. & Sugiura, N., 1987. A kinematic model of TRM acquisition in multidomain magnetite, *Phys. Earth planet. Inter.*, 46, 9–23.
- Menyeh, A. & O'Reilly, W., 1996. Thermoremanent magnetization in monodomain monoclinic pyrrhotite Fe₇S₈, J. geophys. Res., 101, 25 045–25 051.
- Metcalf, M. & Fuller, M., 1987. Domain observations of titanomagnetites during hysteresis at elevated temperatures and thermal cycling, *Phys. Earth planet. Inter.*, **46**, 120–126.
- Moskowitz, B.M. & Halgedahl, S.L., 1987. Theoretical temperature and grain-size dependence of domain state in x = 0.6 titanomagnetite, *J. geophys. Res.*, **92**, 10 667–10 682.
- Néel, L., 1949. Théorie du traînage magnétique des ferromagnétiques en grains fins avec applications aux terres cuites, Ann. Géophys., 5, 99–136
- Néel, L., 1955. Some theoretical aspects of rock magnetism, *Adv. Phys.*, **4**, 191–243.
- Néel, L. & Pauthenet, R., 1952. Étude d'un monocristal de Fe₂O₃-α, C. R. Acad. Sci., Paris, 234, 2172–2174.

- Nishitani, T. & Kono, M., 1983. Curie temperature and lattice constant of oxidized titanomagnetite, *Geophys. J. R. astr. Soc.*, 74, 585–600.
- Özdemir, Ö. & Dunlop, D.J., 2006. Magnetic domain observations on magnetite crystals in biotite and hornblende grains, *J. geophys. Res.*, **111**, B06103, doi:10.1029/2005JB004090.
- Özdemir, Ö. & Dunlop, D.J., 2014. Hysteresis and coercivity of hematite, J. geophys. Res., 119, 2582–2594.
- Özdemir, Ö. & O'Reilly, W., 1981. High-temperature hysteresis and other magnetic properties of synthetic monodomain titanomagnetites, *Phys. Earth planet. Inter.*, 25, 406–418.
- Özdemir, Ö. & O'Reilly, W., 1982. Magnetic hysteresis properties of synthetic monodomain titanomaghemites, *Earth planet. Sci. Lett.*, 57, 437–447.
- Pan, Q., Pokhil, T.G. & Moskowitz, B.M., 2002. Domain structures in epitaxial Fe₃O₄ particles studied by magnetic force microscopy, *J. appl. Phys.*, **91**, 5945–5950.
- Parry, L.G., 1965. Magnetic properties of dispersed magnetite powders, Phil. Mag., 11, 303–312.
- Powell, A.V., Vaqueiro, P., Knight, K.S., Chapon, L.C. & Sánchez, R.D., 2004. Structure and magnetism in synthetic pyrrhotite Fe₇S₈: a powder neutron-diffraction study, *Phys. Rev. B*, 70, 014415.
- Roberts, A.P. et al., 2017. Resolving the origin of pseudo-single-domain behavior, J. geophys. Res., 122, 9534–9558.
- Roberts, A.P., Tauxe, L., Heslop, D., Zhao, X. & Jiang, Z., 2018. A critical appraisal of the "Day" diagram, *J. geophys. Res.*, **123**, 2618–2644.
- Schmidt, V.A., 1973. A multidomain model of thermoremanence, *Earth planet. Sci. Lett.*, **20**, 440–446.
- Schwarz, E.J., 1975. Magnetic properties of pyrrhotite and their use in applied geology and geophysics, Geol. Surv. Can. Paper, 74-59, 24pp.
- Schwarz, E.J. & Vaughan, D.J., 1972. Magnetic phase relations of pyrrhotite, J. Geomag. Geoelec., 24, 441–458.
- Soffel, H., 1977. Pseudo single domain effects and single domain—multidomain transition in natural pyrrhotite deduced from domain structure observations, *J. Geophys.*, **42**, 351–359.
- Stacey, F.D., 1962. A generalized theory of thermoremanence, covering the transition from single domain to multi-domain magnetic grains, *Phil. Mag.*, 7, 1887–1900.
- Stacey, F.D., 1963. The physical theory of rock magnetism, *Adv. Phys.*, **12**, 45–133.
- Stacey, F.D. & Banerjee, S.K., 1974. The Physical Principles of Rock Magnetism, 195pp., Elsevier.
- Sugiura, N., 1981. A new model for the acquisition of thermoremanence by multidomain magnetite, Can. J. Earth Sci., 18, 789–794.
- Sugiura, N., 1988. On the origin of PSD moment in magnetite, *Geophys. J.*, **92**, 479–485.
- Tauxe, L., Bertram, H.N. & Seberino, C., 2002. Physical interpretation of hysteresis loops: micromagnetic modeling of fine-particle magnetite, *Geochem. Geophys. Geosyst.*, 3, 1055, doi:10.1029/2001GC000241.
- Wasilewski, P.J., 1973. Magnetic hysteresis in natural materials, *Earth planet. Sci. Lett.*, **20**, 67–72.
- Wehland, F., Stancu, A., Rochette, P., Dekkers, M.J. & Appel, E., 2005. Experimental evaluation of magnetic interaction in pyrrhotite bearing samples, *Phys. Earth planet. Inter.*, 153, 181–190.
- Xu, S. & Dunlop, D.J., 1994. Theory of partial thermoremanent magnetization in multidomain grains, 2. Effect of microcoercivity distribution and comparison with experiment, *J. geophys. Res.*, 99, 9025–9033.
- Yu, Y., Dunlop, D.J. & Özdemir, Ö., 2002. Partial anhysteretic remanent magnetization in magnetite, 1. Additivity, *J. geophys. Res.*, 107(B10), 2244, doi:10.1029/2001JB001249.
- Yu, Y., Tauxe, L. & Moskowitz, B.M., 2004. Temperature dependence of magnetic hysteresis, *Geochem. Geophys. Geosyst.*, 5(6), Q06H11, doi:10.1029/2003GC000685.